AGU100 ADVANCING EARTH AND SPACE SCIENCE

Space Weather

RESEARCH ARTICLE
10.1029/2018SW002102

Capturing Uncertainty in Magnetospheric Ultralow Frequency Wave Models

S. N. Bentley[1], Clare E. J. Watt[1], I. J. Rae[2], M. J. Owens[1], K. Murphy[3], M. Lockwood[1], and J. K. Sandhu[2]

[1]Department of Meteorology, University of Reading, Reading, UK, [2]Mullard Space Science Laboratory, University College London, Dorking, UK, [3]Department of Astronomy, University of Maryland, College Park, MD, USA

Key Points:
- Determining uncertainty in wave power models is necessary to quantify uncertainty in radial diffusion coefficients for modeling
- Our model of ground-based ULF wave power depends on solar wind speed, number density variance, and B_z; this outperforms hourly persistence
- Total power over extended events is best modeled probabilistically, while the wave power in a single hour is best modeled deterministically

Correspondence to:
S. N. Bentley,
snbentley@outlook.com

Citation:
Bentley, S. N., Watt, C. E. J., Rae, I. J., Owens, M. J., Murphy, K., Lockwood, M., & Sandhu, J. K. (2019). Capturing uncertainty in magnetospheric ultralow frequency wave models. *Space Weather*, *17*, 599–618. https://doi.org/10.1029/2018SW002102

Received 10 OCT 2018
Accepted 28 FEB 2019
Accepted article online 10 MAR 2019
Published online 16 APR 2019

Abstract We develop and test an empirical model predicting ground-based observations of ultralow frequency (ULF, 1–20 mHz) wave power across a range of frequencies, latitudes, and MLT sectors. This is parameterized by instantaneous solar wind speed v_{sw}, variance in proton number density var(Np), and interplanetary southward magnetic field B_z. A probabilistic model of ULF wave power will allow us to address uncertainty in radial diffusion coefficients and therefore improve diffusion modeling of radial transport in Earth's outer radiation belt. Our model can be used in two ways to reproduce wave power: by sampling from conditional probability distribution functions and by using the mean (expectation) values. We derive a method for testing the quality of the parameterization and test the ability of the model to reproduce ULF wave power time series. Sampling is a better method for reproducing power over an extended time period as it retains the same overall distribution, while mean values are better for predicting the power in a time series. The model predicts each hour in a time series better than the assumption that power persists from the preceding hour. Finally, we review other sources of diffusion coefficient uncertainty. Although this wave model is designed principally for the goal of improved radial diffusion coefficients to include in outer radiation belt diffusion-based modeling, we anticipate that our model can also be used to investigate the occurrence of ULF waves throughout the magnetosphere and hence the physics of ULF wave generation and propagation.

Plain Language Summary We construct and test a statistical model for ground-based ultralow frequency wave occurrence, parameterized by solar wind properties. This can be used to find magnetospheric radial diffusion coefficients that determine the transport and energization of electrons in Earth's radiation belts. Our time series prediction outperforms a time series using the assumption that wave power persists from the preceding hour. Using a probabilistic approach reproduces the true distribution of power over extended time periods and is necessary to quantify uncertainty in each step of diffusion modeling.

1. Introduction

Modeling of the outer radiation belt can potentially enable satellite operators to protect their spacecraft from dangerous space weather such as spacecraft charging, deep dielectric charging, and single upset events (Baker et al., 1987; Frederickson, 1996; Horne et al., 2013). One of the areas identified as requiring better characterization in order to improve forecasting and modeling of past events is the radial transport of electrons by ultralow frequency (ULF) plasma waves. This can be achieved by improving models of ULF occurrence, including understanding the azimuthal variation of ULF waves and the underlying coupling to the solar wind (Horne et al., 2013). ULF waves are in the range 1–20 mHz, also known as the Pc 4-5 range following the classification in Jacobs et al. (1964). Frequencies at the lower end of this band are most effective at radial transport, as there is more power on average at lower frequencies (Bentley et al., 2018, Figure 1a) and because lower frequencies can set up drift resonant diffusion (Elkington et al., 1999, 2003). Hence, it is important to examine the generation and propagation of the electromagnetic waves that drive this diffusion and to construct a model of the resultant diffusion that will improve nowcasting and forecasting in the outer radiation belt. Current calculations of radial diffusion coefficients can be constructed from the electromagnetic field in MHD models (Fei et al., 2006) or from observations, either solely using in situ measurements (Lejosne et al., 2013; Liu et al., 2016) or by incorporating ground-based magnetic field

measurements mapped up to the equatorial electric field (Ozeke et al., 2009, 2012, 2014). In situ spacecraft provide more reliable measurements of the electromagnetic waves driving radial diffusion, but spacecraft coverage is sparse and has limited temporal coverage. Ground-based magnetometer networks across the globe have produced many years of observations spanning multiple solar cycles (e.g., Gjerloev, 2012; Mann et al., 2008; Rostoker et al., 1995; Tanskanen, 2009). By mapping these measurements of ULF waves up to the equatorial plane these networks can provide a long-term data set with significantly better spatiotemporal coverage, allowing multiple simultaneous measurements at different locations and encompassing a large range of latitudes (and hence radial locations) and azimuthal (or magnetic local time, MLT) sectors.

Existing models of radial diffusion coefficients are often parameterized by the geomagnetic activity index *Kp* (Ali et al., 2016; Brautigam & Albert, 2000; Lejosne et al., 2013; Ozeke et al., 2014). Individual radial diffusion models based on this parameterization can differ by orders of magnitude (Ali et al., 2016; Liu et al., 2016). This makes it difficult to accurately capture radial diffusion in radiation belt models as the uncertainty in models is unquantified but could easily extend across orders of magnitude. While *Kp* is a proxy for geomagnetic activity, it is not directly related to processes driving ULF waves. Additionally, as a 3-hr-averaged index, only forecasted *Kp* rather than real-time *Kp* can be used for nowcasting or forecasting. The choice of parameters is an important part of constructing any kind of empirical model as the parameters chosen should have a clear physical basis in order to represent (and ultimately to interpret) the physical phenomena underlying the observations. We propose a model based initially on solar wind parameters measured by spacecraft at the L1 Lagrange point, which has a lead time of around an hour (King & Papitashvili, 2005; Richardson & Paularena, 1998; Weimer et al., 2002). The use of solar wind parameters will also represent the external driving of magnetospheric processes by the solar wind and will allow us to directly compare model results to our existing knowledge of those physical processes.

To address the large difference between existing radial diffusion models, we also propose a probabilistic model. In meteorology and climate modeling, probabilistic approaches have met with considerable success in recent years as a method of improving models by accounting for uncertainty and variability in modeling, for example, Berner et al. (2017). Probabilistic models produce a probability distribution as output instead of the single values produced by deterministic models and can be used to quantify the uncertainty introduced by each model component. Model components or steps with larger uncertainty will therefore indicate areas where the model can be improved to better approximate the underlying physics, regardless of the physical process being approximated. Component uncertainties that should be quantified include uncertainty due to initial conditions, boundary conditions, the underlying physics model and (perhaps most importantly for this paper) due to natural internal variability in the system. Probabilistic methods provide a way to quantify variability that either exists naturally or exists due to a parameterization that has yet to be optimized (Watt et al., 2017).

The ultimate goal of this work is to construct a probabilistic model of diffusion coefficients suitable for nowcasting and forecasting. In this article, we focus our initial efforts on outlining a statistical model of ground-based power spectral density (PSD), which can be used to probabilistically predict ULF wave power at the ground from solar wind observations across a range of frequencies, latitudes (i.e., L shells) and azimuthal angles (MLTs). We present the model concept and test it but reserve comparison between the model and physics (i.e., ULF propagation and generation) for future work. In future, this model can also be used to map along field lines to the equatorial plane in the magnetosphere to calculate diffusion coefficients (Ozeke et al., 2009).

In section 2, we briefly review the relationship between ULF PSD and radial diffusion coefficients. In section 3, we present our initial solar wind-based, probabilistic model of ground-based ULF wave power, which is available from the Reading Research Data Archive, Bentley (2019). In section 4, we define what qualities make a "good" parameterization and confirm that our model possesses these qualities. We also test the ability of our solar wind-based model to predict ULF wave power and compare it to a similar *Kp*-based model. In section 5, we discuss other known sources of uncertainty in the calculation of radial diffusion coefficients, in addition to the uncertainty introduced by the underlying description ULF wave power addressed by our model. In section 6, we draw our conclusions and describe future work necessary to apply this initial ULF wave model to the production of diffusion coefficients for radiation belt modeling.

2. ULF Wave Power and Radial Diffusion Coefficients

The Fokker-Planck equation can be used in the outer radiation belt to determine the evolution of a phase space distribution function $\mathcal{F}$ due to diffusion from wave-particle interactions, see, for example, Schulz and Lanzerotti (1974). The most appropriate coordinate system to use is based upon the set of three adiabatic invariants corresponding to quantities conserved in periodic motions of particles trapped in Earth's magnetosphere-gyromotion around a guiding center, bounce motion along the magnetic field between mirror points closer to the Earth and a drift around the Earth itself. We are particularly interested in the case where a disturbance is on a timescale (τ) longer than gyromotion or the bounce period of particles but shorter than or comparable to drift periods ($\tau_{\text{bounce}} << \tau \lesssim \tau_{\text{drift}}$, a range that extends from minutes to hours). This range of timescales corresponds to the periods of ULF waves and impulses such as changes in magnetopause location (Kepko et al., 2002; McPherron, 2005; Southwood & Kivelson, 1990). A disturbance on such a timescale can then lead to a violation of the third adiabatic invariant, while the first two remain conserved. This can result in an increase of kinetic energy for individual particles (see, e.g., Elkington et al., 1999, 2013; Roederer & Zhang, 2014). Additionally, the bulk transport of particles to drift contours closer to (or more distant from) the Earth is particularly of interest when combined with particle sinks and sources. For example, if there exists a source of particles far from the Earth and a sink at low L shell, this mechanism corresponds to a net transport of energy inward. Similarly, when there is a sink at the outer boundary of the magnetosphere, (for example, magnetopause shadowing, Loto'aniu et al., 2010; Turner et al., 2012; West et al., 1972) radial diffusion can result in a loss of energy. Hence, radial diffusion contributes to the energization and transport of particles in the outer radiation belt.

When considering only third-invariant diffusion, the diffusion equation reduces to

$$\frac{\partial \mathcal{F}}{\partial t} = L^{*2} \frac{\partial}{\partial L^*} \left[\frac{1}{L^{*2}} D_{LL} \frac{\partial \mathcal{F}}{\partial L^*} \right] \tag{1}$$

(Roederer & Zhang, 2014; Schulz & Lanzerotti, 1974) with radial diffusion coefficient

$$D_{LL} = \frac{\langle (\Delta L^*)^2 \rangle}{2\tau}, \tag{2}$$

where $L^* = \frac{2\pi B_E R_E^2}{\phi}$ (Roederer & Zhang, 2014). Hence, L^* is related to the third adiabatic invariant, namely, flux ϕ through a drift contour, and is related to the equatorial radius r_0 of the corresponding drift contour in a dipole with no field perturbations. This is clear using units of Earth radii, ($L^* = r_0/R_E$). While the drift shell radius will change once the dipole field is distorted, the L^* value will be conserved. Calculating the mean square displacement in L^*, $(\Delta L^*)^2$, reduces to an integral whose nonnegligible terms use the autocorrelation of electromagnetic field amplitudes (Fälthammar, 1965, 1968; Fei et al., 2006; Lejosne et al., 2012). The Fourier transform of the autocorrelation function and PSD are related via the Wiener-Khinchin theorem, assuming a weakly stationary and stochastic signal. Hence, PSD at each frequency is an important component of D_{LL} (Fälthammar, 1965; Fei et al., 2006; Schulz & Lanzerotti, 1974). Typically, for radiation belt modeling $(\Delta L^*)^2$ is estimated using electric and magnetic ULF wave PSDs (Ali et al., 2016; Brautigam & Albert, 2000; Brautigam et al., 2005; Fei et al., 2006; Liu et al., 2016; Ozeke et al., 2012, 2014).

This work focuses on constructing a statistical model of ULF PSDs that can quantify the uncertainty passed forward into ULF wave-derived radial diffusion coefficients. However, there are multiple other sources of uncertainty in our diffusion coefficient calculations that are reviewed in section 5. These other sources can arise from physical assumptions used in our formalism, from restrictions imposed by observation methods, or from statistical methods in creating models.

3. Model Construction

In this section, we discuss the method of construction of a statistical map of ground-based ULF wave power, parameterized by physical properties that have been demonstrated to causally correlate with power (Bentley et al., 2018; "Paper 1"). Here "causally correlated properties" are properties whose correlation to ULF power cannot be attributed to covariance with other solar wind parameters. The probabilistic model we outline can be used to estimate the uncertainty in predictions of ULF wave PSDs. We will show that the conditional probability distributions resulting from this parameterization can be approximated by a family of normal distributions whose mean and variance values make a good parameterization. We discuss possible uses and

Table 1
Parameters Used to Discretely Partition Model

Parameter	Values	Num. values
Radial L shell (station latitude)	Four stations FCHU, GILL, ISLL, PINA ($L \sim 7.94, 6.51, 5.40, 4.21$)	4
Frequency	0.83–20 mHz	69
Azimuthal angle (MLT)	Dawn, noon dusk, and midnight (3–9, 9–15, 15–21, and 21–3 MLT)	4
$B_z = 0$ threshold	$B_z > 0$ and $B_z < 0$	2

Note. These parameters define the separate partitions. Solar wind properties $v_{sw}, B_z < 0, \mathrm{var}(Np)$ are used in each partition to parameterize the power observed.

testing of such a probabilistic model, and in future, we also intend to use this to investigate the underlying physics of ULF generation and propagation.

To construct this statistical wave map, we use the data as detailed in Paper 1; solar wind observations from National Aeronautics and Space Administration/Goddard Flight Center's OMNI data set through OMNIWeb at http://omniweb.gsfc.nasa.gov/ and ground-based magnetic field measurements from the CANOPUS magnetometer chain in Canada (Rostoker et al., 1998; now upgraded and expanded to form CARISMA [Canadian Array for Realtime Investigations of Magnetic Activity], Mann et al., 2008) to calculate PSD in hourly windows from 1990–2005 using the multitaper method. This conserves the square of the signal in the time (t) and frequency (f) domain as follows:

$$\sum_f PSD(f) = \Delta t \sum_t |x(t)|^2 = \int_{t=0}^{T} |x(t)|^2 \mathrm{d}t, \tag{3}$$

where $x(t)$ is the detrended signal in the time domain and Δt the time resolution.

Previous work (Paper 1) has identified three near-instantaneous solar wind properties that are causally correlated with ULF PSD: solar wind speed v_{sw}, interplanetary magnetic field $B_z < 0$, and summed perturbations in number density across 1.69–6.79 mHz, δN_p. The method used to identify these properties accounts for skewed data distributions and solar wind interparameter relationships by deconvolving the contribution of each individual solar wind parameter to ground ULF wave power from the relationship with other correlated solar wind parameters. Hence, these solar wind properties are each directly related to the occurrence of ULF wave power. In this paper, we demonstrate the construction of a parameterization using the three solar wind parameters above, with the expectation that further parameters such as geomagnetic activity, magnetospheric plasma density distribution, substorms, time lags, and history of the magnetosphere will be added as necessary in future. In this work, we choose to use $\mathrm{var}(N_p)$ in place of δN_p as it is equivalent in the analysis method of Paper 1 but is simpler to use.

3.1. Partitions of the Magnetosphere

To capture the changing behavior of ULF waves in different regions of the magnetosphere, we define a set of nested bins. We call the magnetospheric bins "partitions," which depend on frequency, azimuthal angle (i.e., MLT), and radial location (i.e., L shell, defined by station latitude). These are reviewed in Table 1. The parameterization using three solar wind properties is performed separately in each partition, so that our final empirical model is dependent on the solar wind, the region of the magnetosphere, and ULF frequency. For the remainder of this article, "bins" will solely refer to the nested solar wind parameter bins nested in each partition. We choose to cover frequencies from 0.8 to 20 mHz. Lower frequencies contain the most power but as the power tends to drop off gradually with frequency (Bentley et al., 2018, Figure 1a), we also include higher frequencies in order to examine their contribution. The data set is already discretized by radial location and frequency (due to the use of different ground magnetometer stations and our PSD calculation), and we subdivide the data further into four MLT sectors centered at dawn, noon, dusk, and midnight. Use of four sectors allows us to resolve azimuthal variations while retaining enough data to construct a parameterization. In addition, we split the data at $B_z = 0$ as Paper 1 indicates that the physical processes either driving or propagating ULF waves differs for $B_z > 0$ and $B_z < 0$. This will aid future analysis of the physics. The full L shell ranges corresponding to the four magnetometer stations FCHU, GILL, ISLL, and PINA over this time period can be found in Table 1 of Rae et al. (2012).

Therefore, in total, we have $4 \times 69 \times 4 \times 2 = 2,208$ partitions. In each of these, we parameterize ULF wave power using $v_{sw}, B_z < 0$, and $\mathrm{var}(Np)$ bins. In this paper, we present and test the results of the ground-based

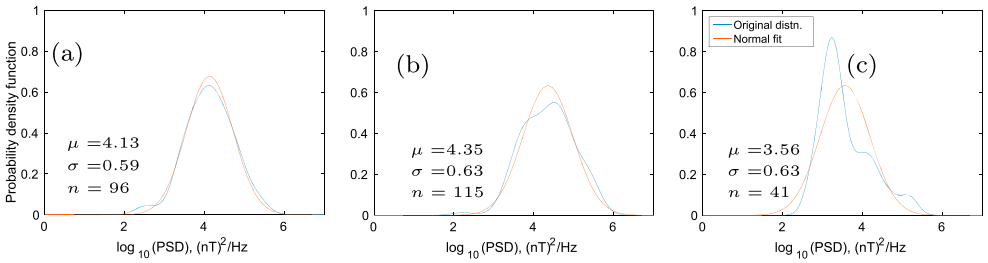

Figure 1. The original and normal (fitted) distributions of log power in three example bins from the GILL station at $L \sim 6.6R_E$, 3.33 mHz, with $B_z < 0$ in the noon sector; the three distributions most likely (a), highly unlikely (b), and least likely (c) to be drawn from a normal distribution, with chi-square p values of $p = 0.95, 0.13, 0.01$, respectively. Bin (a) is centered at $v_{sw} = 558$ km/s, $\log_{10}(\text{var}(Np)) = -0.059$ cm^{-3}, $B_z = -1.23$ nT; (b) is centered at 608 km/s, -0.999 cm^{-3} and -1.23 nT, and (c) is centered at 407 km/s, 0.620 cm^{-3}, and -1.23 nT. For each bin, the mean μ and standard deviation σ of the distribution of the n points in that bin are shown. PSD = power spectral density.

geomagnetic north-south component in order to validate our approach. The east-west component is also included in the data set. Together, these comprise the magnetospheric toroidal and poloidal modes (Elkington, 2013) plus some mixing. The final, perpendicular component represents the compressional mode and is not included.

3.2. Parameterization in Each Partition

The model in each partition is constructed by binning ground-based ULF wave power by the corresponding solar wind properties. We remove the 0.1% most extreme solar wind values to improve data resolution, (i.e., the lowest and highest 0.05% values). This results in a parameter space where the end bins are not unnecessarily large and empty. The relevant ranges are velocity: 282 to 783 km/s, variance of proton number density: 0.0038 to 42.814 cm^{-3}, and B_z: −12.3 to 11.5 nT. From this point onward, we use $\log_{10}(\text{var}(N_p))$ instead of var(Np) in order to work with linear scales in our parameterization. Bins are equally spaced on this linear scale and are the same in each partition.

In any one partition (i.e., for one station, MLT sector, frequency and for $B_z <$ or > 0), we determine conditional probability distributions of ULF wave power given observations of solar wind properties v_{sw}, $\log_{10}(\text{var}(Np))$ and B_z. We bin observed power into a $10 \times 10 \times 5$ grid and examined the distribution of $\log_{10}(PSD)$ in each bin. Since we split at $B_z = 0$, the B_z dimension only has five bins instead of 10. For each partition, this creates a 3-D lookup table of probability distributions that are parameterized by the solar wind observations. These are therefore conditional probability distributions as they express the probability distribution given a particular set of solar wind properties.

The distribution of $\log_{10}(PSD)$ in each bin is approximated with a normal distribution, by fitting a normal to the log power observed in each bin containing at least 10 points. While the majority of bins contain distributions of log power that are technically statistically distinct from normal distributions, they are nonetheless reasonable approximations. In Figure 1, we show example distributions from three bins in a single partition; a probability distribution that is highly likely to be drawn from a normal distribution as measured using a chi-square goodness of fit test (Figure 1a) and two others that are far less likely (Figure 1b) and highly unlikely (Figure 1c). While all three may not be exactly normally distributed, this makes a reasonable approximation, with the arguable exception of Figure 1c. However, even for this poor fit, a normal approximation is preferable to having nothing in this bin. The poor fit of Figure 1c indicates how uncertainty can enter PSD prediction when underlying approximations (here the lognormal assumption) are less valid. Examining where these fits are good approximations is an example of the future analysis that can be done to investigate the physics, as the type of distribution may provide insight into the underlying physical processes.

Constructing a distribution for each bin in a given partition provides multiple benefits compared to simply taking the mean or median; first, if we choose to use the mean or median in future, we retain information about the range and variance. Second, we are able to then use these distributions for probabilistic forecasting. We note that as the distribution in each bin describes the occurrence of ULF wave PSD depending on the solar wind conditions, this is a set of conditional probability distribution functions, which allows us to explore the physics of ULF occurrence in new ways. By approximating these probability distributions as

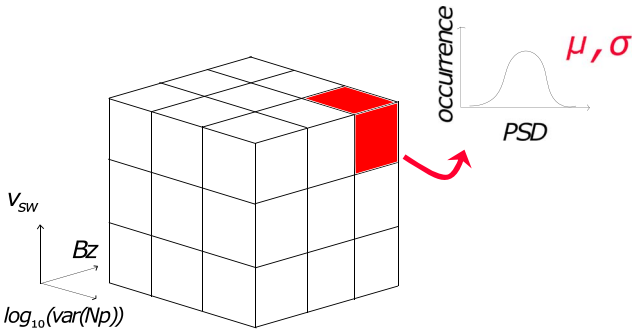

Figure 2. A visualization of our parameterization for each station, magnetic local time sector, and frequency partition. Using a 3-D grid with solar wind speed, variance of proton number density, and interplanetary magnetic field axes, ground-measured ULF wave log power is binned and the corresponding probability distributions (a family of normal distributions) are used to model the power. We use 10, 10, and 5 bins for each solar wind parameter, respectively, in the model. PSD = power spectral density.

lognormals, we can use this information relatively cheaply, as for every single bin in a given partition, we need only store the mean and variance of each normal distribution of log power rather than the entire distribution.

3.3. Example: Using This Model

We have produced a series of lookup tables which, for each partition (station/freq/MLT/Bz < or > 0), contain a family of normal distributions parameterized by the near-instantaneous solar wind properties. Figure 2 illustrates this; we can use the bins nested in each partition to look up the distribution function of ULF PSD values for a given solar wind speed, variance of proton number density, and B_z observed in the solar wind (i.e., conditional probability distribution functions). Hence, at each point in time, this model can be used in two ways; given the solar wind observations, we can look up the corresponding conditional probability distribution and either use the expectation value (i.e., the mean) of the distribution or sample the entire distribution. Sampling will randomly obtain PSD values drawn from the probability distribution in a given bin. With many such samples, the distribution of our predicted values will converge toward the original distribution in that bin. In this way, a time series of reproduced power can then be built up an hour at a time, either deterministically (i.e., using the mean) or stochastically (by sampling).

An example reproduced hourly time series is shown in Figure 3 where we show the solar wind speed v_{sw}, variance in number density $\log_{10}(\mathrm{var}(Np))$, B_z, and the original and reproduced log power measured at GILL station, 3.33 mHz, for 2 weeks in May 2001. We also show the number density Np for reference. The reproduced power shown in (e) can be found by using the mean values in each lookup table (orange) or by sampling. For the sampling method, 2,000 time series were constructed and for each hour in Figure 3 the blue sleeve indicates the the interquartile range of samples taken. This time period was chosen for the variety of solar wind speed conditions; however, the few gaps in our reproduction also highlight some areas of our model that can be improved. These gaps are primarily due to data gaps in the solar wind observations in variance of number density (absent $\sim$ 15% of the time from 1990–2005 when OMNI data are supplied for v_{sw}, Bz) and also due to too few observations in the more extreme bins, preventing us from determining the underlying probability distribution. We anticipate that these will be addressed using additional solar wind observations and/or Np correlations for the former, and additional years of data and/or extrapolations for the latter. More simply, approximations could be made using only v_{sw} and Bz. In Figure 3e, it can be seen that the observed and reproduced log power roughly follow each other. Overall the model appears to have performed exceedingly well given that it depends primarily on the instantaneous contribution of three solar wind properties and includes no time lags or properties internal to the magnetosphere. There appears to be a diurnal variation that is captured reasonably well by the four MLT sectors used here; the relative contribution of the solar wind parameters and MLT sectors to the PSD observed throughout the magnetosphere will be considered in future work. However, first, we must verify that our model is a good approximation to the original PSD observations. We discuss different metrics for testing this model below.

4. Testing the Model

While the ability to reproduce observed phenomena is an important test of a model, other model qualities determine whether it is fit for purpose and whether it produces statistically significant results. We discuss all these qualities first, before building metrics in section 4.2 to measure the ability of our model to reproduce ULF wave power observations and comparing to a similar Kp-based model in section 4.3.

4.1. Characterizing a Good Parameterization

We use the following criteria to define a good parameterization, in no particular order:

1. The parameterization reproduces behavior well, as measured by a relevant metric.

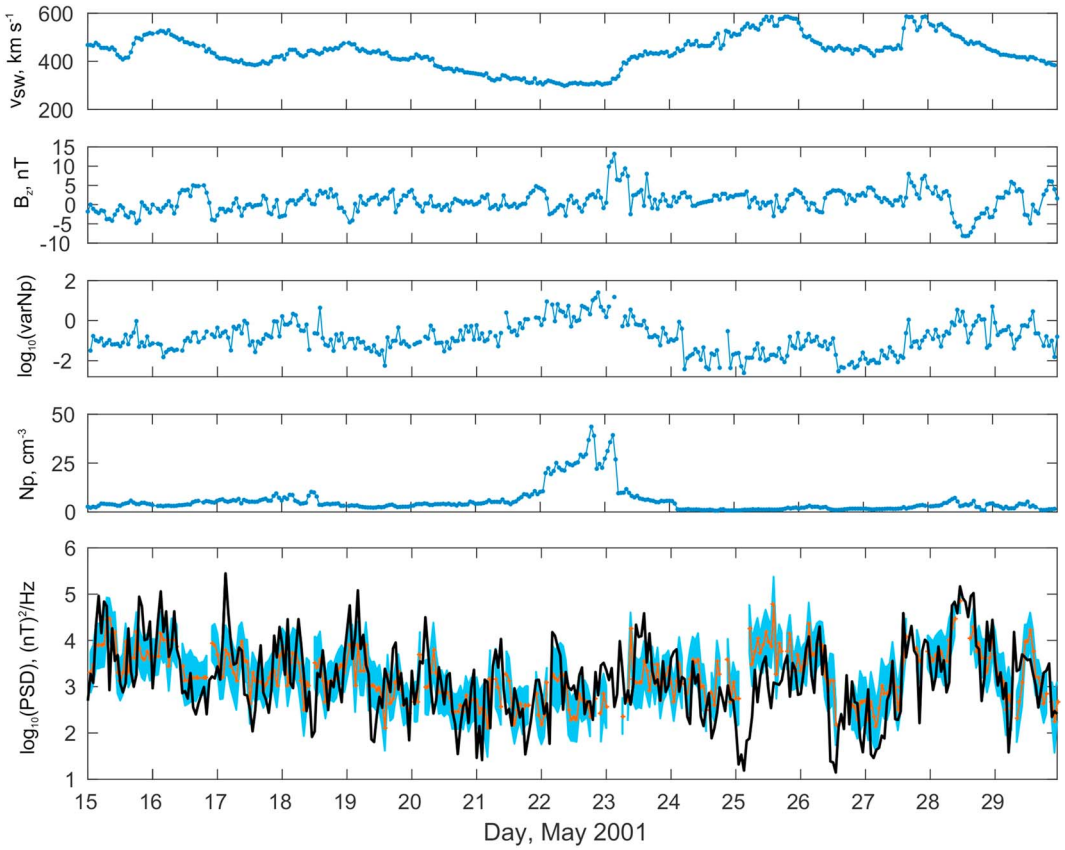

Figure 3. Using instantaneous solar wind speed v_{sw} (a), southward interplanetary magnetic B_z (b), and variance in proton number density $\log_{10}(\mathrm{var}(Np))$ (c), the power spectral density observed across all MLT sectors at a single station and frequency (GILL, 3.33 mHz) can be reproduced using a family of normal probability distributions parameterized by solar wind properties. (e) The original power time series (black) and power reproduced using our model, either by taking the mean of the probability distribution given the observed solar wind values (orange) or by sampling from that distribution multiple times (the interquartile range of 2,000 samples is shown in blue). (d) The proton number density in the solar wind for reference. PSD = power spectral density.

2. Parameters chosen are significantly related to changes in PSD, that is, the probability distribution of power values in neighboring bins are distinct. Variance is minimized, while the mean values are much larger and vary more.
3. Parameters are physically motivated, and we can interpret their impact.
4. The parameterization can be used for nowcasting and forecasting.
5. Excess parameters are excluded to avoid overfitting, as models with larger degrees of freedom are less statistically significant.

The ability of our model to reproduce observed PSD values is examined in section 4.2. The importance of the second criterion is illustrated in Figures 4a and 4b; the larger the variance in each bin, the more likely that neighboring probability distributions overlap. This is a consequence of our finite amount of data, which in turn can only be binned by a finite number of parameters. With infinite data, considerable overlap would be fine and we could bin by all physically motivated parameters. Instead, when we can only use a finite number of parameters a clear evolution of PSD distribution across neighboring bins suggests that the parameters chosen are significantly related to changes in PSD. Numerous overlap coefficients exist to examine the relationship between two normal distributions, but we can define a simple metric here specifically to quantify how this overlap affects the quality of our parameterization. This metric is particularly suitable as the standard deviation of all our bins are so similar (discussed below). We use the ratio of the standard deviation in

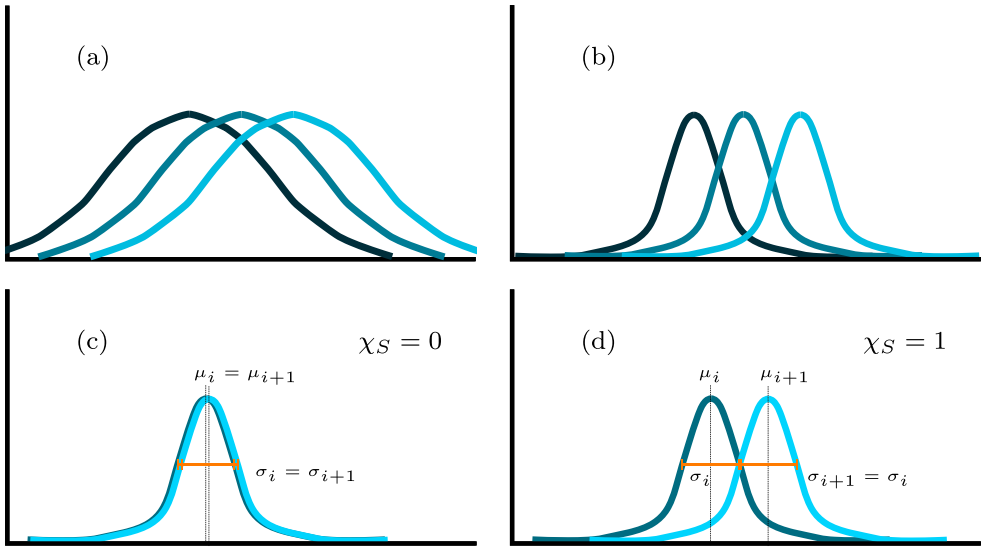

Figure 4. (a, b) An illustration of two sets of three normal distributions, which have the same three mean values but a larger (a) and smaller (b) variance. We would consider (b) a better parameterization as there is considerably more overlap between neighboring probability distributions in (a). (c, d) The distribution overlap corresponding to separation proxy values of 0 and 1, respectively, when the standard deviations of each distribution are roughly the same.

each bin to the difference in mean values; for two neighboring bins, b_i and b_{i+1}, this quantity is then the separation proxy

$$\chi_S = \frac{\|\mu_i - \mu_{i+1}\|}{\langle \sigma_{i,i+1} \rangle}, \tag{4}$$

which (as illustrated in Figures 4c and 4d) will be 0 for two completely overlapping distributions but will be equal to 1 for two distributions with equal standard deviations, where the point of overlap is exactly one standard deviation of either mean. The median values of this separation proxy between all neighboring bins for GILL, 3.33 mHz, noon, $Bz < 0$ is 0.5 for probability distributions along the speed axis, 0.28 along $\log_{10}(\text{var}(Np))$, and 0.37 along Bz. For GILL, 3.33 mHz, noon, $Bz > 0$, these values are 0.6, 0.29, and 0.25, respectively. The magnitude of these values corresponds to the order of dominant contributing parameters v_{sw}, $Bz < 0$, and var(Np) as expected and indicate that in future such a measure can be used to investigate where the solar wind parameters contribute meaningfully to changes in ULF power.

This separation proxy χ_S is very similar to the well-established effect size measure Cohen's d (Cohen, 1988). Instead of standardizing the two mean values by the average standard deviation $< \sigma_{i,i+1} >$, Cohen's d standardizes by the "pooled" standard deviation that weights by the number of points in each distribution. This is unnecessary here as the normal distributions are already known to be approximations, and the uncertainty arising from that approximation should be decoupled from our separation proxy and investigated separately. However, we note that in the case where $\sigma_i = \sigma_{i+1}$, much of the existing literature on interpreting Cohen's d can still be applied here.

Indeed, the separation proxy χ_S is most meaningful where the standard deviations of all distributions are roughly the same; hence, a more detailed comparison of mean and standard deviation (μ, σ) values is made for all bins at GILL, 3.33 mHz in Figure 5. Figure 5a shows the distribution of all σ values, which is clustered around ~ 0.7. This can be compared to Figure 5b, which shows the σ of normal distributions fitted to the same number of power values that were randomly selected from the original distribution rather than using our binning technique. (This was run 1,000 times). As the variance is smaller for our parameterization, our model is outperforming randomly selected distributions. Figure 5c shows the μ values for GILL, 3.33 mHz, corresponding to the σ shown in Figure 5a. This range of mean values indicates that the mean power (i.e., PSD, not $\log_{10}(PSD)$) varies over several orders of magnitude, while the variance of each distribution is about an order of magnitude for each bin. Hence, the family of probability distributions we use is better than randomly selected distributions as the variance is smaller, and the variance/mean ratio is such that changes in the solar wind parameters correspond to the probability distribution shifting up and down the power axis

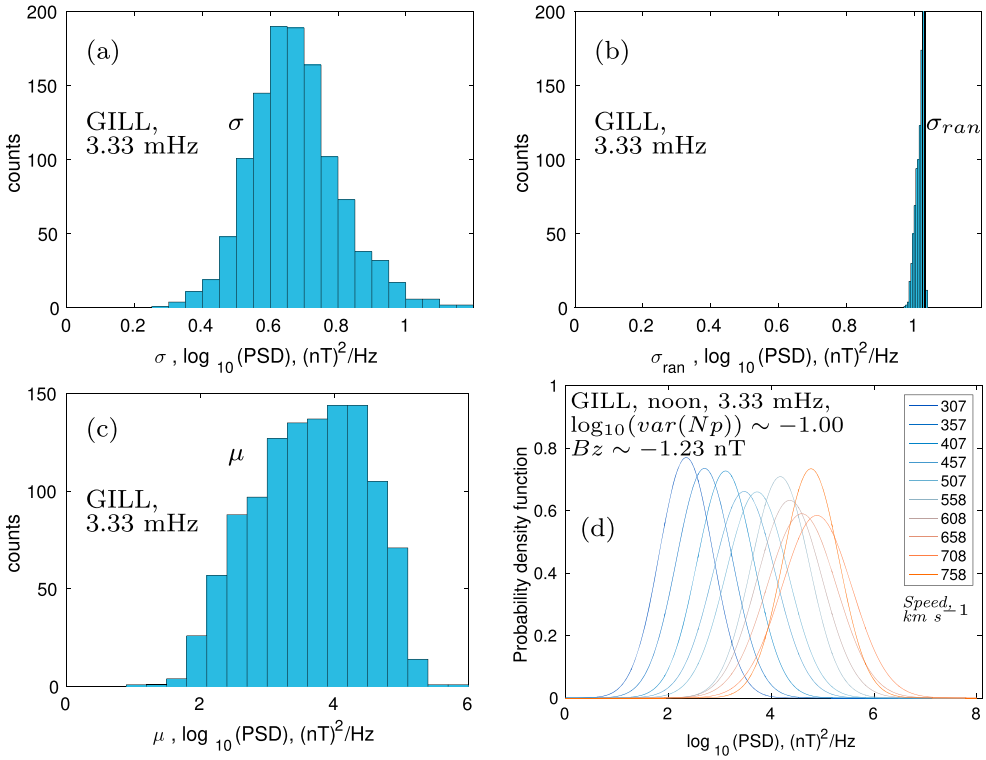

Figure 5. (a) The standard deviation (σ) values of the normal fitted probability distributions for all bins at GILL, 3.33 mHz. (b) The σ values of normal distributions fitted to bins of equal size as those in (a) but randomly sampled from the original distribution. (c) The mean (μ) values of the normal probability distributions, corresponding to those in (a). There is less variance in each probability distribution when binning by three solar wind parameters than in equivalent randomly sampled distributions, and this variance is small and consistent relative to the range of mean values. (d) An example of the variation of probability distributions with speed in a constant Bz, var(Np) bin in a single partition. PSD = power spectral density.

without changing shape. An example of this can be seen in Figure 5d; the probability distributions associated with different solar wind speed values for constant Bz, var(Np) bin is shown for GILL, 3.33 mHz in the noon sector, $Bz < 0$. For lower solar wind speeds the distributions are distinct, while at higher speeds they overlap. Future improvements of this parameterization could involve identifying where such distributions should be merged using χ_S, while identifying what this corresponds to physically is one example of the future work that can be done to understand the underlying physics using this probabilistic model.

Criteria 3 and 4 reflect the intention that our model be capable of investigating existing physics and, eventually, be capable of forecasting. For a model parameterizing radial diffusion coefficients, the chosen parameters should also be clearly and significantly related to changes in the diffusion coefficients. The solar wind parameters used in this model were selected as they have been shown to be causally correlated to ground ULF wave power; a review of their physical interpretation can be found in Paper 1. As they are drawn from solar wind observations they can be used for nowcasting and forecasting. We have attempted to reduce the degrees of freedom by only using causally correlated solar wind parameters and by using a long time period, which makes overfitting on the five parameters here (L,MLT, v_{sw}, Bz, var(Np)) unlikely.

4.2. Ability to Predict ULF Wave Power

We anticipate that our model will be put to two main uses: calculating the total power distribution over an extended event or predicting the power for each hour in a time series. For example, the total distribution method will be useful for long timescale reconstructions where it is important to reproduce signal properties that include the overall distribution, while the time series will be useful for forecasting. Both outputs may be useful to case studies of individual events. Therefore, we examine the efficacy of this model using two tests. The first (a series of violin plots) compares the total distribution of log power from the original observed log power to the distribution of log power reproduced from our model. The second test (forecasting skill)

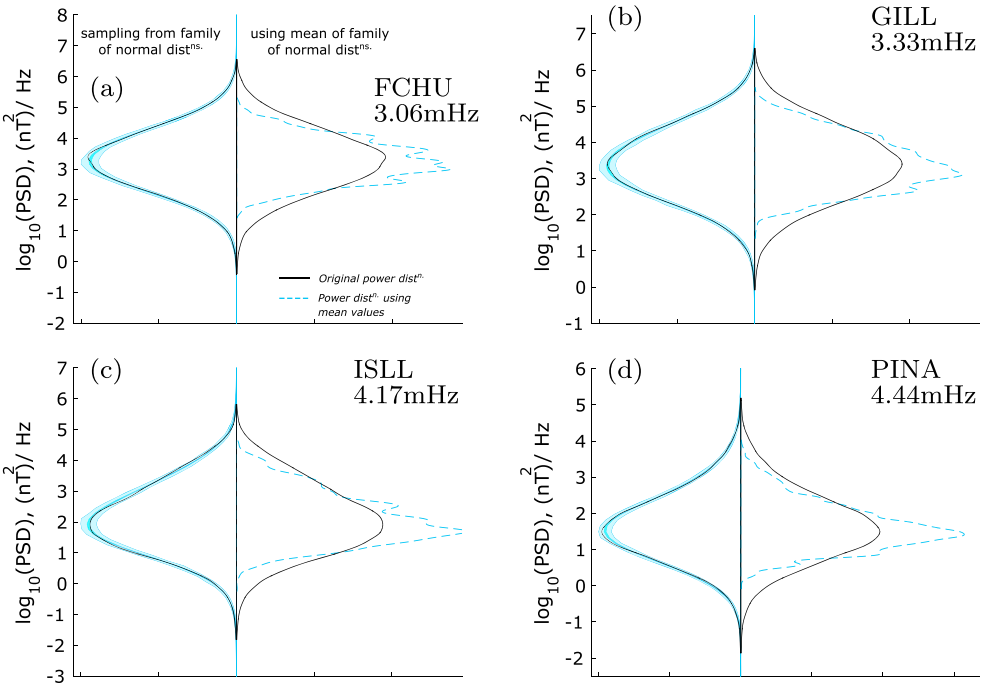

Figure 6. Violin plots showing the probability distribution of power over the original 15 years of data, compared to reproduced distributions of power using the two methods possible with our model. For each hour, the model defines a probability distribution of power that is dependent on solar wind conditions; this is used to reproduce the original 15-year distribution. The left-hand side of each violin compares the original total power distribution to the reproduced distribution found by sampling from the conditional probability distribution of power for each hour, while the right-hand side compares to taking the mean value of the conditional probability distribution for each hour. Black lines indicate the original distribution, while the reproduced values are indicated by a dashed blue line (mean values), a blue region (interquartile range of 2,000 samples), and light blue region (upper and lower bounds from sampling). This is shown for four combinations of station and frequency. Violins are all scaled so that the area under the original and reproduced distributions are equal to 1. PSD = power spectral density. PSD = power spectral density.

examines the ability to predict power in the oncoming hour compared to a reference model. Both these tests are completed first on sample partitions of the entire 15 years of original data and on a small set of CARISMA data from January–March 2015, that is, we test our model on both the training data and on data outside the training window. Customarily, such testing is not done on training data; however, the size of the data set compared to the few parameters we have used suggests that this is a reasonable test.

We use vertically plotted probability distribution functions (violin plots) in Figure 6 to compare original and reproduced probability distributions of PSD over an extended time. Here we have chosen four representative combinations of station and frequency; the frequency for each station is the average eigenfrequency over all MLT as calculated by the cross-phase technique (Sandhu et al., 2018; Waters et al., 1991) over several years. Hence, this is a stricter test than choosing consistently "quiet" frequencies for each station. For each combination the total original power distribution (black) is compared to reproduced power using the mean of each probability distribution (right, blue) and to sampling from the probability distributions (left, blue). As the original distribution falls roughly between the interquartile range when using the sampling method, but is clearly very far off for the means method, this suggests that a sampling method is suitable for obtaining the power distribution over an extended event while the mean is not. Interestingly, PINA and FCHU appear to have the worst fits, which may be due to the changing plasmapause and magnetopause locations crossing these respective stations. This is an example of the latitude- and MLT-dependent physics we intend to explore in future. Unfortunately, it is very difficult to statistically quantify the ability to reproduce these distributions without overly favoring either the center of the distribution or the tails; we have been unable to find a suitable metric. Existing measures designed to measure the similarity of two distributions found our sampled reproductions to be either all very good or all very poor. Therefore, future study is necessary to

Table 2
Forecasting Skill at Selected Stations and Frequencies

	Model skill score vs. random reference model			
Partition tested	24-hr Persistence	1-hr Persistence	Model (sampled)	Model (means only)
FCHU, 3.06 mHz	34.9	69.1	48.7	74.6
GILL, 3.33 mHz	38.0	74.1	55.6	78.0
ISLL, 4.17 mHz	37.6	76.2	56.5	78.4
PINA, 4.44 mHz	35.3	72.7	54.8	77.6

Note. Forecasting skill scores for four stations and frequencies, testing the ability of the solar wind parameterized model to reproduce the original 15 years of data. The baseline reference model used is a "random" model, where power is sampled from the original total distribution of the given partition. Simple 24- and 1-hr "persistence" models are tested against this baseline (i.e., assuming power in the oncoming hour is the same as the previous day or hour) in addition to the solar wind-parameterized model. The probability distributions predicted for each hour by the solar wind model were either sampled or the mean value was taken to construct each 15-year time series. Where sampling methods were used, 2,000 time series were made and the forecast skill calculated for each one; the median is shown here.

identify a metric that accurately reflects our ability to reproduce the physical distributions and that can be used as a tool to improve our model by distinguishing where fits are good or bad.

Forecasting skill is a simple measure that can be used to compare the ability of two methods to predict a time series. In space physics, it has previously been used to test solar wind predictions, for example, Owens et al. (2013). It is calculated as follows:

$$Skill = 100\left(1 - \frac{MSE_{\text{model}}}{MSE_{\text{ref}}}\right), \tag{5}$$

using the mean square error (*MSE*) between each model and the observed values. Forecast skill scores can range from $-\infty$ to 100 and positive values indicate that the tested model is better than the reference model. We compare both mean and sampling methods of applying our model and two "persistence" models to a random model sampling from the entire original distribution of power, as per Owens et al. (2013). The two persistence models assume that the power we see in the next hour will be the same as that observed 24 hr ago and 1 hr ago, respectively. Calculating forecasting skill is relatively simple using the means or persistence method as the reproduced time series is always the same. To calculate forecasting skill for random and sampling methods, 2,000 time series were constructed by sampling from either the random or appropriate normal distributions. The forecasting skill was calculated for each of these time series and the median forecasting skill of these 2,000 runs taken. Results of this are shown in Table 2.

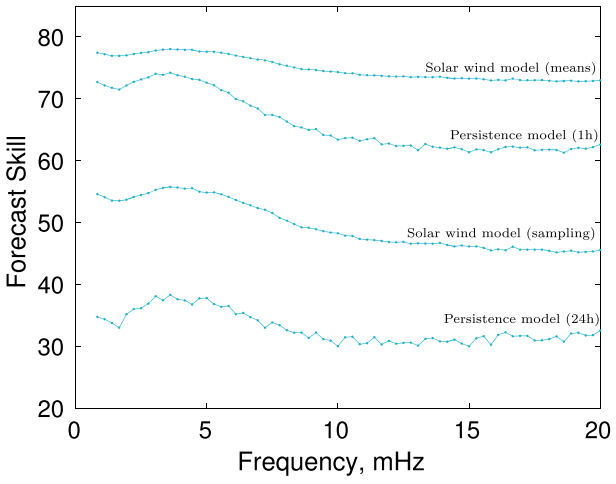

Figure 7. Forecasting skill at all frequencies for GILL, 1990–2005, where models are compared to a random reference model. Where any kind of sampling was used (i.e., random and solar wind model sampling), 500 runs were taken. The ranking of model types is consistent across all frequencies.

For all four examples, both means and sampling methods of using our model were better than randomly sampling, as expected. However, both methods were also superior to assuming 24-hr persistence and using the expected (mean) value from our lookup tables is a better predictor of power than assuming that power continues from the previous hour. For example, at FCHU 3.06 mHz, all four models tested are better than the baseline "random" model as they all have positive values. With the highest forecasting skill score of 74.6, using the mean values of each parameterized probability distribution outperforms all other models, followed by 1-hr persistence with a score of 69.1. Sampling from the probability distributions lags behind this with a skill score of 48.7 and 24-hr persistence performs least well with a score of 34.9. To confirm that this ranking is not frequency dependent, we have also calculated forecasting skill across 1990–2005 for every frequency at a single station (GILL) using a smaller number of runs, shown in Figure 7. Across all frequencies, the ranking of models compared to a random reference model remains

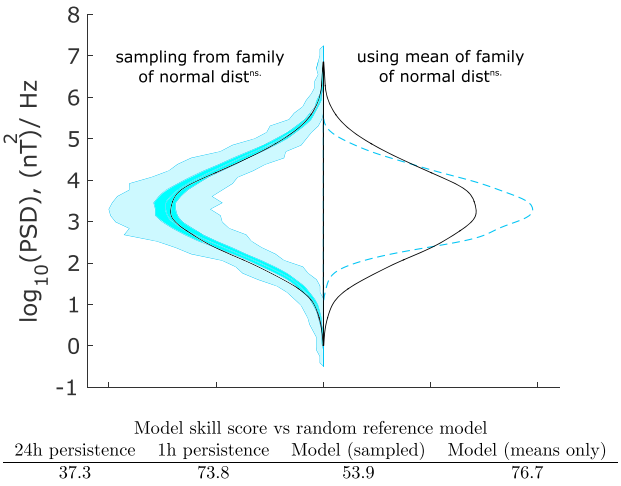

Figure 8. Testing the ability of a solar wind-parameterized model to predict ground-based power not in our training set, across January–March 2015, GILL, 3.33 mHz. The violin plot compares both the sampled and mean-value methods against the original total power distribution over an extended time period (as in Figure 6), and the forecasting skill tests the ability of models to reproduce a time series. Here we compare the performance of two persistence models and our solar wind-parameterized model (using both sampling and the mean methods) to a baseline "random" model, as described in Table 2. Results are very similar to the tests carried out on the training data; the sampling method reproduces the power distribution well (as the original power lies within the interquartile range of reproductions), while the mean value predicts the oncoming hour best. PSD = power spectral density.

the same. Hence, using the mean value is the best method for reproducing a time series, whereas the sampling method is outperformed by 1-hr persistence. However, it should be recalled that the sampling method outperformed the mean method for reproducing the total distribution (as tested using violin plots in Figure 6). Therefore, different construction methods should be used depending on the desired output.

Similarly, we test these methods for 3.33 mHz at GILL using CARISMA data for January–March 2015 in Figure 8. Again, the sampling method is best for reproducing the total power distribution over these 2 months, and the mean method is superior at predicting the power in individual hours. Note that while the sleeve between the upper and lower bounds in the violin plot of Figure 8 is wider than in Figure 6, this is a slightly misleading visualization artifact due to plotting less populated distributions, as the CARISMA data is considerably shorter. It is more important to note that the original power distribution shown in black still lies within the interquartile range of our samples. This emphasizes the need for a metric that quantifies the ability of the model to reproduce total power distributions rather than relying on visualizations.

4.3. Comment on Other Possible Parameters

The parameters used so far correspond to three near-instantaneous solar wind properties and the radial and azimuthal location in the magnetosphere. Therefore, there is no history of the solar wind or the magnetosphere, including the persistence of existing ULF waves. The method presented in this paper does not represent internal properties such as substorm activity or magnetospheric plasma density; therefore, our current distributions average over all internal configurations. This is likely to contribute to the variance in each distribution and requires further study. While no internal parameters or geomagnetic indices are included, we compare our results to a *Kp*-based model below. Finally, our selection of parameters includes no long-term dependencies, such as seasonal or solar cycle variations. It has long been understood that ULF wave activity varies with solar activity phase (Murphy et al., 2011; Saito, 1969). An underlying assumption of this work is that such effects can be characterized by the changing solar wind parameters v_{sw}, Bz, var(Np) rather than representing this changed solar output indirectly using a parameter such as F10.7. As the magnetospheric mass density also varies over a solar cycle, once internal properties have been included, the ability of our chosen parameters to represent ULF wave power changes across a solar cycle could be compared to F10.7. More sophisticated methods will be necessary to add further parameters as we cannot further reduce the number of data points in each bin.

4.4. Comparison to *Kp*-Based Models

Existing models of radial diffusion coefficients and ULF wave PSD use *Kp*. We cannot compare directly to the values predicted by the *Kp*-parameterized ground-based empirical model of Ozeke et al. (2014) as our prototype model describes ground-based power instead of total power in the equatorial azimuthal field. Instead, we can briefly examine the properties of a *Kp*-based model of ground PSD, constructed similarly to the solar wind model already presented. Ground-based PSD at 3.33 mHz, GILL is binned by the corresponding *Kp* value and the probability distribution function is calculated in each bin. These distributions are shown in Figure 9a. By merging overlapping high *Kp* bins, a parameterization could be constructed where the distributions are distinct with relatively small variance. Hence, a *Kp*-based model based on sampling empirical probability distribution functions could be constructed that satisfies point 2 of the necessary conditions for a good parameterization in section 4.2. However, it would not fully satisfy the requirement for forecasting or nowcasting capability (due to the 3-hr-averaged nature of *Kp*) or the requirement for physically motivated parameters (it is difficult to ascribe a direct physical property to *Kp* due to the processing involved in constructing it, as discussed below). The variance of the *Kp* bins are similar to those in our solar wind-parameterized model (Figure 5); there may be a lower limit to the variance, either dependent on our hourly timescale or due to underlying physical processes that require better characterization.

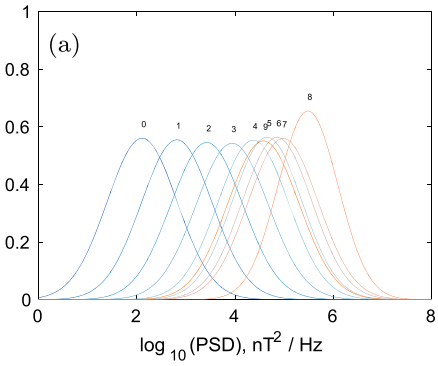

(b)

Kp	μ	σ
0	2.11	0.71
1	2.81	0.72
2	3.42	0.73
3	3.94	0.73
4	4.37	0.72
5	4.65	0.71
6	4.85	0.71
7	4.98	0.71
8	5.48	0.61
9	4.57	0.72

(c)

Kp	μ_S	σ_S
0	2.16	0.84
1	2.79	0.78
2	3.47	0.83
3	3.86	0.80
4	4.33	0.81
5	4.55	0.81
6	4.60	0.88
7	4.97	0.93
8	5.20	1.10
9	n/a	n/a

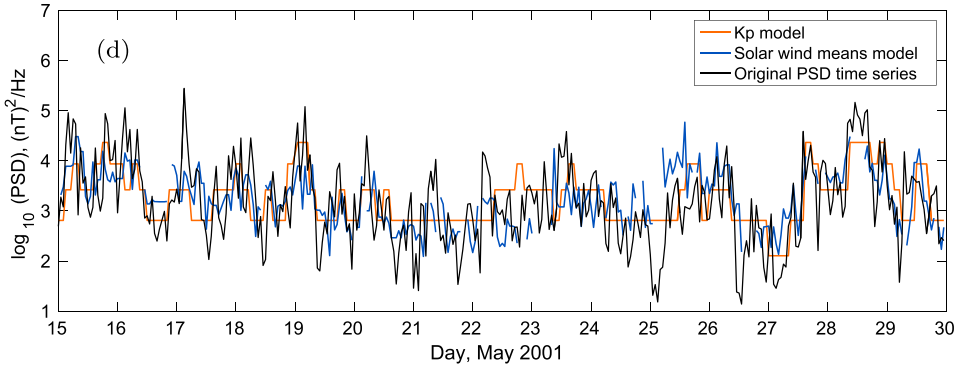

Figure 9. A *Kp*-based model using probability distributions to predict ultralow frequency wave power at GILL, $L \sim 6.6$, 3.33 mHz. (a) The fitted normal distributions of power for each *Kp* values, (b) the mean and standard deviation of both these fits, and (c) similar storm time only fits. In (d), we use both the *Kp* and solar wind parameter models to reproduce power over a short period of time (2 weeks in May 2001, the same as Figure 3). PSD = power spectral density.

Interestingly, the variance of each *Kp* bin in this model (explicitly shown in Figure 9b) is clearly smaller than those from the storm time data set used by Murphy et al. (2016), even while the mean values are similar. The storm list used by Murphy et al. (2016) is based on times where the magnetosphere is driven by corotating interaction regions and coronal mass ejections, although part of the list was also constructed with a *Dst* threshold. The greater uncertainty in the storm time values (i.e., the larger variance) is therefore likely to be caused by more extreme solar wind conditions, while the similarity in the mean values is most likely due to either a correlation between *Dst* and *Kp*, to the fact that a portion of the storm list does not use a *Dst* threshold and so the internal conditions of the magnetosphere may not be significantly different to the average or most probably a combination of the two. Regardless of the similar mean values, the increase in uncertainty indicates that *Kp* does not capture ground ULF wave power behavior as well under extreme solar wind conditions. It is likely that our model will perform better, being solar wind based, but future work should quantify this.

To compare the *Kp*-based model directly to our solar wind based model, we have used the *Kp* probability distribution functions to reproduce PSD values for the same time series as Figure 3, shown in Figure 9d. The time series is reasonably well followed by both models, but forecasting skill scores indicate that the *Kp* model does not perform quite as well as our solar wind based model. At GILL over the 15 years, for 3.33 mHz the solar wind-based model has a positive skill value of 10.6 when compared to *Kp* as a reference model. Nevertheless, *Kp* is a surprisingly good proxy for ground-based PSD. Examining the relationship between *Kp* and the solar wind parameters suggests that *Kp* represents an independent contribution to power; the two-parameter plot in Figure 10 shows that median PSD increases with *Kp* independently of v_{sw}, *Bz*, or $\log_{10}(\mathrm{var}(Np))$. (This analysis is in line with that followed in Paper 1 to identify causally correlated parameters.) As *Kp* is a midlatitude index, it is related to the magnetospheric convection electric field (Thomsen, 2004), while as a range index it is particularly related to explosive changes such as substorms. Since it is a 3-hr index and substorm cycles generally last within 3 hr (Borovsky & Yakymenko, 2017), *Kp* is therefore related to substorm activity (Lockwood, 2013). However, very large amplitude ULF waves may also contribute to *Kp*, as they may cause significant magnetic field deviations on the dayside stations used to construct *Kp*,

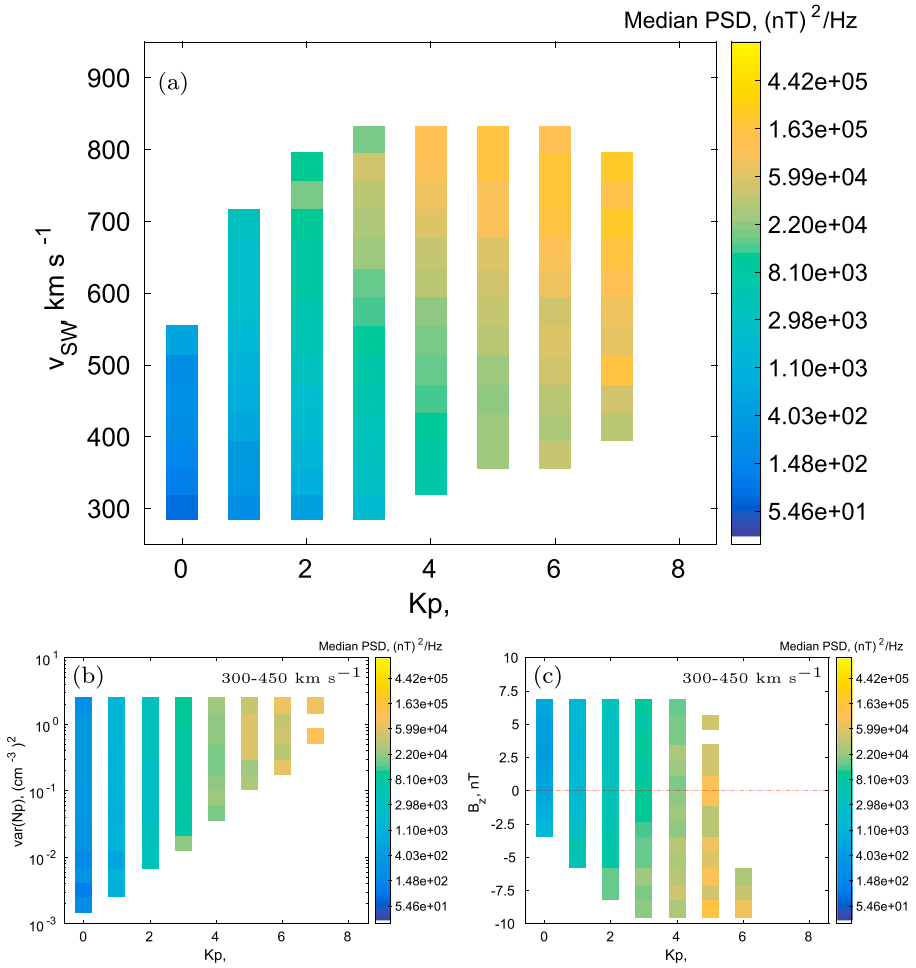

Figure 10. A series of "two-parameter" plots, where observations are binned by a solar wind parameter and *Kp*, and the median power in each bin at GILL, 3.33 mHz is shown. (a) Power is binned by both speed and *Kp*. Median ultralow frequency (ULF) wave power is shown, which increases with both parameters. (b) Power is binned by variance in proton number density *Np* and *Kp* for a single speed bin. Median ULF wave power increases with *Kp* but not with variance in number density. (c) Power is binned by *Bz* and *Kp* for a single solar wind speed. Median ULF wave power increases with both $Bz < 0$ and *Kp*. Hence, *Kp* represents a contribution to median ULF wave power independent of any correlations with solar wind speed, *Bz*, or variance in proton number density. PSD = power spectral density.

particularly during times of low substorm activity. Hence, the independent contribution indicated by *Kp* may represent substorm activity or ULF wave persistence. This suggests that ULF wave persistence should be studied and that one of the first improvements to this prototype model should account for internal magnetospheric processes such as substorm activity. However, as *Kp* is highly averaged and processed, suitable options would be either a more physically based internal parameter, a solar wind time lag, or the recent history of the magnetosphere. These different approaches will need to be considered for both their physical interpretability and their suitability for nowcasting and forecasting.

5. Other Sources of Uncertainty in Radial Diffusion Coefficients

In this paper, we have focused on a model of ULF wave PSD that will allow us to quantify the uncertainty introduced to calculation of radial diffusion coefficients. However, to construct a probabilistic description of diffusion coefficients, we will need to include all sources of uncertainty; in this section, additional sources of uncertainty are reviewed. Physical assumptions used in our theoretical formalism, constraints due to observational capabilities and different statistical methods all contribute to this uncertainty. Indeed, some sources of uncertainty have multiple knock-on effects such as the underlying magnetic field model, which can give

rise to uncertainty in the formalism and again when calculating L^*, that is, in processing observational data and when constructing averages for statistical wave maps.

The following review is ordered from purely physical assumptions, through approximations of theory that make up our formalism, to observational restrictions and finally uncertainty from our statistical model construction.

1. Background magnetic field model
2. Other physics underlying the formalism
3. Summation over resonant frequencies
4. Accounting for azimuthal wave structure
5. Double-counting symmetric perturbations
6. Double-counting electric field perturbations
7. Methods of calculating PSD
8. Uncertainty from ground- and space-based observations
9. Statistical method construction

This list of known sources of uncertainty are all briefly reviewed below.

5.1. Background Magnetic Field

As discussed in section 2, the diffusion coefficient D_{LL} can be derived from perturbations of electromagnetic fields. Fälthammar (1965) considered the radial diffusion of equatorially mirroring particles due to small symmetric and asymmetric perturbations of the dipole field, while others have extended this to other magnetic field models (Elkington et al., 2003; Schulz & Eviatar, 1969). Clearly, the choice of magnetic field model will contribute some uncertainty to the resulting diffusion coefficients, particularly at higher radial distances and during geomagnetically extreme periods when magnetic field models are often less accurate. This choice also gives rise to uncertainty in using observations, as we map in situ observations from real space to L^* or ground-based observations up to the equatorial plane.

5.2. Other Physics Underlying the Formalism

Diffusion coefficients are bounce-averaged and hence calculated in the equatorial plane, using equatorially mirroring particles. This assumes that there is no latitude-dependent field variation such as the South Atlantic Anomaly. Additionally, the radial diffusion coefficient used in radiation belt modeling is generally drift averaged. However, there is no conventional method of constructing a drift-averaged diffusion coefficient as it is unclear whether it is more physically representative to calculate D_{LL} in each azimuthal sector and average or to calculate $(\Delta L^*)^2$ in each sector, average these and then calculate D_{LL}. Instead, the lack of simultaneous measurements across a wide range of MLT sectors often dictates our choice. Finally, we also note for completeness that an underlying physical assumption used in these derivations is that the frozen-in theorem is valid, that is, that there is no parallel electric field (Falthammar, 1968).

5.3. Summation Over Resonant Frequencies

Radial diffusion coefficients for a particle of a given energy are found in many existing formulations by evaluating the power at frequencies corresponding to the resonant and harmonic drift frequencies of a particle (Ali et al., 2016; Brautigam et al., 2005; Fei et al., 2006; Ozeke et al., 2014). An example of this mechanism can be found by Elkington et al. (1999). They showed that global toroidal mode ULF oscillations can accelerate electrons, particularly with the addition of a dawn-dusk electric field. However, integrating over a broader frequency range than just resonant frequencies results in larger final diffusion coefficients via a sum of smaller scatterings, where this frequency range is determined by the drift frequency and the sampling frequency (up to the bounce frequency limit; Lejosne et al., 2013). Hence, clarifying the role of resonant and nonresonant diffusion will be necessary to understand the energy dependence of diffusion coefficients.

When using the resonant frequency method, a common assumption used is that radial diffusion is caused by a magnetic impulse similar to a step function, so that power decays very slowly and is proportional to inverse square frequency, $P \propto f^{-2}$ (Ozeke et al., 2014; Schulz & Lanzerotti, 1974). This assumption is particularly useful as it causes the energy dependence of D_{LL} to cancel out and hence makes the diffusion coefficient easier to calculate. This approximation appears to be valid for average power spectra but may not hold for the spectrum in an individual hour.

5.4. Accounting for Azimuthal Wave Structure

Using observations to calculate D_{LL} via a sum over drift resonances involves yet more uncertainty in using and determining wave structures from in situ observations. Where our formalism sums only over resonant frequency contributions, we must estimate the power at harmonics of that frequency. In their radial diffusion coefficient derivation, Fei et al. (2006) use a sum over azimuthal mode numbers m to describe this effect. However, in practice, this is often simplified by assuming $m = 1$. Sarris and Li (2017) found that the amplitude of power is indeed concentrated in low m numbers for the dayside and for less geomagnetically active time periods but less so for the nightside and geomagnetically active periods. Murphy et al. (2018) found that the m number during a moderate storm is typically low but the distribution of positive or negative values depends on radial location; this initial study gives some idea how the direction of propagation (i.e., $m <$ vs. > 0) is distributed among ULF waves but due to challenges in measuring m much more work is required. It is also unclear how direction of propagation should be included in existing radial diffusion coefficient calculations, yet the orientation of these oscillations will clearly affect the resultant diffusion.

5.5. Double-Counting Symmetric Perturbations

Another source of uncertainty that comes into both the theoretical framework and when using observations is double counting from background magnetic field perturbations. This arises from the inclusion of both symmetric and asymmetric magnetic field perturbations, when only asymmetric (i.e., azimuthally dependent or varying in MLT) variations contribute to radial diffusion (Fälthammar, 1965; Lejosne et al., 2012, 2013). While axisymmetric variations in the magnetic field may distort the entire drift contour (hence moving particles in real space) particles will not be moved to a new drift contour (i.e., changing the value of enclosed flux or L^*) without asymmetric perturbations. Observationally, it is difficult to identify asymmetric components from in situ data as it is generally a set of sparsely located point measurements, yet the asymmetric component is of smaller amplitude at the ground where there is better coverage of observations. This difficulty was resolved by Lejosne et al. (2012, 2013), who avoid the issue of confusing symmetric with asymmetric perturbations by using an analytical model of disturbances added to a dipole field. By sampling multiple in situ locations, the value of these additional terms can be determined. Lejosne et al. (2013) also describes a method to approximate this type of analysis using only single point measurements, which reduces the number of spacecraft coverage necessary to cover the L^* shells and sectors of interest. While this approach removes symmetric double counting, uncertainty remains from the use of a dipole field model. This emphasizes the necessity of calculating uncertainty to allow us to choose between physical assumptions in diffusion coefficient estimation methods.

5.6. Double-Counting Electric Field Perturbations

The second type of double counting arises from our treatment of electric fields. Theoretically, if the inductive electric field term is neglected from the magnetic component of diffusion D_{LL}^B, adiabatic changes in the magnetic field may appear to result in spurious changes in L^* and hence in our radial diffusion coefficients (Fälthammar, 1965). However, it is difficult to quantify this term as in situ observations simply provide the localized value of the electric field, and it is difficult to distinguish how much of that is due to induction (i.e., $\frac{dB}{dt}$). Hence, any diffusion coefficient calculation is at risk of double-counting electromagnetic field contributions. Using the method briefly mentioned in the previous section, Lejosne et al. (2012, 2013) also address this inductive electric field double counting. More commonly, simplifying assumptions are made to make this problem more tractable. Fei et al. (2006) simply sum the electric and magnetic components $D_{LL} = D_{LL}^E + D_{LL}^B$. This approach is approximately valid where either the two electric components can be distinguished, (for example, by making assumptions on the background magnetic field model and the types of wave present, which determines the relationship between the electric and magnetic field perturbations, Ozeke et al., 2012) or when either $D_{LL}^E << D_{LL}^B$ or $D_{LL}^B << D_{LL}^E$. However, these coefficients may be of comparable magnitude (Pokhotelov et al., 2016), so it is unclear how often this approximation can be used.

5.7. Methods of Calculating PSD

While PSD is vital to our diffusion coefficient derivations, there are multiple valid transforms between the time and frequency domain. Different transform methods are better suited for either broadband or narrowband signals and so may over or underestimate the power at a single frequency; hence, the choice of transform should reflect either the drift-resonant sum or frequency-range integral method of coefficient derivation. For example, if D_{LL} is calculated at specific resonant frequencies, then different methods of calculating PSD could result in different amounts of diffusion. Additionally, the underlying assumptions of a transformation to the frequency domain via the Wiener-Khinchin theorem have not been fully explored,

such as stationarity on a range of timescales. It is not clear whether this would contribute uncertainty to the final diffusion coefficients but is included here for completeness.

5.8. Uncertainty From Ground- and Space-Based Observations

Some types of uncertainty are unique to the observation method. While the real-space location of in situ data may be known, it is difficult to be certain of the L^* value. Spacecraft are often located at the equator and therefore may be at the node of any resonant field line oscillations, which they will therefore underestimate. As point measurements, it is difficult to make assumptions about the spatial and temporal scale of oscillations from single spacecraft measurements. However, ground-based data have their own set of uncertainties; each ground station corresponds to some field line-centered volume of variable width, and the mapping of ground power to the equatorial plane relies on assumptions of ionospheric conductivity and number density variations along the field, in addition to the magnetic field model and $E_{||} = 0$ approximations discussed previously (Ozeke et al., 2009).

5.9. Statistical Model Construction

When constructing statistical models of diffusion coefficients, additional uncertainty enters due to our methods of averaging and parameterization. For example, while azimuthal resolution is important for statistical wave maps as it is the asymmetric (azimuthally dependent) contributions that account for radial diffusion, it is unclear what size azimuthal sector to average over as the spatial coherence of ULF waves has not been studied for this purpose. Similarly, the plasma density distribution affects the occurrence and penetration of ULF waves and hence radial diffusion. Averaging over periods with both high and low densities will introduce more variability in statistical models.

Finally, the method of constructing a statistical model can also introduce uncertainty by our choice of parameters. Several recent studies calculating diffusion coefficients across the magnetosphere parameterize by *Kp* and *L* (Ali et al., 2016; Brautigam & Albert, 2000; Brautigam et al., 2005; Lejosne et al., 2013; Liu et al., 2016; Ozeke et al., 2014). Using *L* as a parameter is fraught with difficulty due to the difficulty mapping *L* to L^*. The quality of such a parameterization can be quantified by examining the fits and the choice of parameters, as discussed in section 4.1.

5.10. Summary

There are many sources of uncertainty in our existing methods of calculating diffusion coefficients. Quantifying the uncertainty introduced by different theoretical formalisms and by different physical assumptions will aid in selecting the most appropriate model approach with minimal uncertainty. Uncertainty due to observational restrictions, underlying natural variation, and due to statistical methods may not be as easily avoided but still needs to be quantified in order to accurately describe the ability of radial diffusion coefficients to reproduce radiation belt phenomena in modeling. In this paper, we have focused on producing a statistical model of ULF PSD that is suitable for nowcasting and forecasting yet can capture the uncertainty due to underlying natural variation. This is only one component of a final, fully probabilistic radial diffusion coefficient model. Until then, it can be used to improve existing models and to better understand the physics underlying the generation and propagation of ULF waves.

6. Conclusion

A description of ULF wave power is an important component of any radial diffusion coefficient calculation. We have outlined a method to construct a model of ground-based ULF wave power that is dependent on solar wind parameters, azimuthal angle (i.e., MLT), station latitude, and frequency. This model outputs probability distributions, which will allow us to produce probabilistic forecasts and to identify areas of uncertainty in future statistical models of radial diffusion coefficients.

The probability distribution in each bin is approximated by a normal distribution of log power, which allows us to use two methods of predicting ULF wave power. By looking up the appropriate normal distribution corepsonding to solar wind observations in a given hour, that distribution can either be sampled or the mean can be taken. Sampling each distribution is suitable for reproducing the total distribution of power over an extended event, while using the mean value is the best method of reproducing a time series. Comparing this to a similarly constructed model based on *Kp*, we find that our prototype model based only on three solar wind parameters slightly outperforms the *Kp* model and that *Kp* represents an independent contribution to power that should later be included in our model. We also find that the uncertainty in a *Kp* parameterization

increases during storm times. Hence, future improvements could include a dependence on internal magnetospheric properties that satisfy the characteristics of a good parameterization, which we have defined in section 4.1.

To apply this prototype model to the production of radial diffusion coefficients involves extending to more stations and mapping ground based power to the equatorial electric field (Ozeke et al., 2009, 2012), then examining whether this is an effective model and where the largest uncertainty stems from. Identifying the source of this uncertainty will allow for targeted improvement of a statistical radial diffusion coefficient model. In section 5, we reviewed other ways that uncertainty can enter the radial diffusion coefficient calculation in addition to the underlying wave model. We anticipate that the methods and tests outlined throughout this paper can be used to inform construction of other components of a fully probabilistic radial diffusion coefficient model.

Future improvements to reduce any uncertainty from the solar wind-based model outlined here could be made by including time-lagged solar wind contributions, substorms, magnetospheric plasma density, magnetospheric conditions, and also the time history of the magnetosphere. Additionally, the underlying normal distribution approximation could be further examined to identify where this approximation holds; as well as quantifying the resulting uncertainty, this will indicate magnetospheric regions or solar wind conditions of physical interest for the generation and propagation of ULF waves.

To summarize, our simple parameterization based on magnetospheric regions and just three solar wind properties predicts ULF wave power time series better than assuming that power carries on from the previous hour. We submit that this is a surprisingly effective result for such a simple model and therefore constitutes a step toward a probabilistic model of radial diffusion coefficients. This prototype model can also be used to investigate questions about the occurrence of ULF waves; immediate future work includes examining the parameterization results across a variety of stations and MLT sectors.

Acknowledgments
The authors gratefully acknowledge use of NASA/GSFC's Space Physics Data Facility OMNIWeb service and OMNI data and the use of data from the CANOPUS/CARISMA magnetometer array (www.carisma.ca), which is operated by the University of Alberta and funded by the Canadian Space Agency. S. N. B. receives funding from the Natural Environment Research Council as part of the SCENARIO Doctoral Training Partnership NE/L002566/1. C. E. J. W. is supported by STFC grant ST/R000921/1 and NERC grant NE/P017274/1. I. J. R. is supported by NERC grant NE/P017185/1 and STFC grant ST/N000722/1. M. J. O. and M. L. are supported by STFC consolidated grant ST/M000885/1 and the SWIGS NERC Directed Highlight Topic Grant NE/P016928/1/. K. R. M. is partially funded by NSF grant 1602403, and J. K. S. is supported by STFC consolidated grant ST/N0007722/1 and NERC grant NE/L007495/1. The authors would like to thank additional members of the NERC Rad-Sat consortium for useful discussions, and S. N. B. would like to thank Solène Lejosne for discussions that refined this work. The statistical model constructed using the methods outlined in this article is available from the University of Reading Research Data Archive (https://doi.org/10.17864/1947.190).

References

Ali, A. F., Malaspina, D. M., Elkington, S. R., Jaynes, A. N., Chan, A. A., Wygant, J., & Kletzing, C. A. (2016). Electric and magnetic radial diffusion coefficients using the Van Allen Probes data. *Journal of Geophysical Research: Space Physics*, *121*, 9586–9607. https://doi.org/10.1002/2016JA023002

Baker, D. N., Belian, R. D., Higbie, P. R., Klebesadel, R. W., & Blake, J. B. (1987). Deep dielectric charging effects due to high-energy electrons in Earth's outer magnetosphere. *Journal of Electrostatics*, *20*(1), 3–19. https://doi.org/10.1016/0304-3886(87)90082-9

Bentley, S. N. (2019). A probabilistic, empirical model of magnetospheric ultra-low frequency wave power. University of Reading Research Data Archive. (dataset, https://doi.org/10.17864/1947.190).

Bentley, S. N., Watt, C. E. J., Owens, M. J., & Rae, I. J. (2018). ULF wave activity in the magnetosphere: Resolving solar wind interdependencies to identify driving mechanisms. *Journal of Geophysical Research: Space Physics*, *123*, 2745–2771. https://doi.org/10.1002/2017JA024740

Berner, J., Achatz, U., Batté, L., Bengtsson, L., De La Cámara, A., Christensen, H. M., et al. (2017). Stochastic parameterization toward a new view of weather and climate models. *Bulletin of the American Meteorological Society*, *98*(3), 565–587. https://doi.org/10.1175/BAMS-D-15-00268.1

Borovsky, J. E., & Yakymenko, K. (2017). Substorm occurrence rates, substorm recurrence times, and solar wind structure. *Journal of Geophysical Research: Space Physics*, *122*, 2973–2998. https://doi.org/10.1002/2016JA023625

Brautigam, D. H., & Albert, J. M. (2000). Radial diffusion analysis of outer radiation belt electrons during the October 9, 1990, magnetic storm. *Journal of Geophysical Research*, *105*(A1), 291–309. https://doi.org/10.1029/1999JA900344

Brautigam, D. H., Ginet, G. P., Albert, J. M., Wygant, J. R., Rowland, D. E., Ling, A., & Bass, J. (2005). CRRES electric field power spectra and radial diffusion coefficients. *Journal of Geophysical Research*, *110*, A02214. https://doi.org/10.1029/2004JA010612

Cohen, J. (1988). *Statistical power analysis for the behavioral sciences* (2nd ed.). Hillsdale, NJ: Erlbaum.

Elkington, S. R. (2013). A review of ULF interactions with radiation belt electrons. In P. J. Kazue Takahashi, R. E. D. Chi, & R. L. Lysak (Eds.), *Magnetospheric ULF waves: Synthesis and new directions* (pp. 177–193). Washington, DC: American Geophysical Union. https://doi.org/10.1029/169GM12

Elkington, S. R., Hudson, M. K., & Chan, A. A. (1999). Acceleration of relativistic electrons via drift-resonant interaction with toroidal-mode Pc-5 ULF oscillations. *Geophysical Research Letters*, *26*(21), 3273–3276. https://doi.org/10.1029/1999GL003659

Elkington, S. R., Hudson, M. K., & Chan, A. A. (2003). Resonant acceleration and diffusion of outer zone electrons in an asymmetric geomagnetic field. *Journal of Geophysical Research*, *108*(A3), 1116. https://doi.org/10.1029/2001JA009202

Fälthammar, C.-G. (1965). Effects of time-dependent electric fields on geomagnetically trapped radiation. *Journal of Geophysical Research*, *70*(11), 2503–2516. https://doi.org/10.1029/JZ070i011p02503

Falthammar, C.-G. (1968). Radial diffusion by violation of the third adiabatic invariant. In B. McCormac (Ed.), *Earth's particles and fields, Proceedings of the NATO Advanced Study Institute, July 31–August 11* (Vol. 1967, pp. 157–169). Chicago, IL: Reinhold Book Corporation.

Fei, Y., Chan, A. A., Elkington, S. R., & Wiltberger, M. J. (2006). Radial diffusion and MHD particle simulations of relativistic electron transport by ULF waves in the September 1998 storm. *Journal of Geophysical Research*, *111*, A12209. https://doi.org/10.1029/2005JA011211

Frederickson, A. R. (1996). Upsets related to spacecraft charging. *IEEE Transactions on Nuclear Science*, *43*(4), 2454. https://doi.org/10.1109/TNS.1996.531795

Gjerloev, J. W. (2012). The SuperMAG data processing technique. *Journal of Geophysical Research*, *117*, A09213. https://doi.org/10.1029/2012JA017683

Horne, R. B., Glauert, S. A., Meredith, N. P., Boscher, D., Maget, V., Heynderickx, D., & Pitchford, D. (2013). Space weather impacts on satellites and forecasting the Earth's electron radiation belts with SPACECAST. *Space Weather*, *11*, 169–186. https://doi.org/10.1002/swe.20023

Jacobs, J. A., Kato, Y., Matsushita, S., & Troitskaya, V. A. (1964). Classification of geomagnetic micropulsations. *Geophysical Journal of the Royal Astronomical Society*, *8*(3), 341–342. https://doi.org/10.1029/JZ069i001p00180

Kepko, L., Spence, H. E., & Singer, H. J. (2002). ULF waves in the solar wind as direct drivers of magnetospheric pulsations. *Geophysical Research Letters*, *29*(8), 1197. https://doi.org/10.1029/2001GL014405

King, J. H., & Papitashvili, N. E. (2005). Solar wind spatial scales in and comparisons of hourly Wind and ACE plasma and magnetic field data. *Journal of Geophysical Research*, *110*, A02104. https://doi.org/10.1029/2004JA010649

Lejosne, S., Boscher, D., Maget, V., & Rolland, G. (2012). Bounce-averaged approach to radial diffusion modeling: From a new derivation of the instantaneous rate of change of the third adiabatic invariant to the characterization of the radial diffusion process. *Journal of Geophysical Research*, *117*, A08231. https://doi.org/10.1029/2012JA018011

Lejosne, S., Boscher, D., Maget, V., & Rolland, G. (2013). Deriving electromagnetic radial diffusion coefficients of radiation belt equatorial particles for different levels of magnetic activity based on magnetic field measurements at geostationary orbit. *Journal of Geophysical Research: Space Physics*, *118*, 3147–3156. https://doi.org/10.1002/jgra.50361

Liu, W., Tu, W., Li, X., Sarris, T., Khotyaintsev, Y., Fu, H., et al. (2016). On the calculation of electric diffusion coefficient of radiation belt electrons with in situ electric field measurements by THEMIS. *Geophysical Research Letters*, *43*, 1023–1030. https://doi.org/10.1002/2015GL067398

Lockwood, M. (2013). Reconstruction and prediction of variations in the open solar magnetic flux and interplanetary conditions. *Living Reviews in Solar Physics*, *10*, 4. https://doi.org/10.12942/lrsp-2013-4

Loto'aniu, T. M., Singer, H. J., Waters, C. L., Angelopoulos, V., Mann, I. R., Elkington, S. R., & Bonnell, J. W. (2010). Relativistic electron loss due to ultralow frequency waves and enhanced outward radial diffusion. *Journal of Geophysical Research*, *115*, A12245. https://doi.org/10.1029/2010JA015755

Mann, I. R., Milling, D. K., Rae, I. J., Ozeke, L. G., Kale, A., Kale, Z. C., et al. (2008). The upgraded CARISMA magnetometer array in the THEMIS era. *Space Science Reviews*, *141*, 413–451. https://doi.org/10.1007/s11214-008-9457-6

McPherron, R. L. (2005). Magnetic pulsations: Their sources and relation to solar wind and geomagnetic activity. *Surveys in Geophysics*, *26*(5), 545–592. https://doi.org/10.1007/s10712-005-1758-7

Murphy, K. R., Inglis, A. R., Sibeck, D. G., Rae, I. J., Watt, C. E. J., Silveira, M., et al. (2018). Determining the mode, frequency and azimuthal wave number of ULF waves during a HSS and moderate geomagnetic storm. *Journal of Geophysical Research: Space Physics*, *123*, 6457–6477. https://doi.org/10.1029/2017JA024877

Murphy, K. R., Mann, I. R., Rae, I. J., & Milling, D. K. (2011). Dependence of ground-based Pc5 ULF wave power on F10.7 solar radio flux and solar cycle phase. *Journal of Atmospheric and Solar-Terrestrial Physics*, *73*(11–12), 1500–1510. https://doi.org/10.1016/j.jastp.2011.02.018

Murphy, K. R., Mann, I. R., Rae, I. J., Sibeck, D. G., & Watt, C. E. J. (2016). Accurately characterizing the importance of wave-particle interactions in radiation belt dynamics: The pitfalls of statistical wave representations. *Journal of Geophysical Research: Space Physics*, *121*, 7895–7899. https://doi.org/10.1002/2016JA022618

Owens, M. J., Challen, R., Methven, J., Henley, E., & Jackson, D. R. (2013). A 27 day persistence model of near-Earth solar wind conditions: A long lead-time forecast and a benchmark for dynamical models. *Space Weather*, *11*, 225–236. https://doi.org/10.1002/swe.20040

Ozeke, L. G., Mann, I. R., Murphy, K. R., Jonathan Rae, I., & Milling, D. K. (2014). Analytic expressions for ULF wave radiation belt radial diffusion coefficients. *Journal of Geophysical Research: Space Physics*, *119*, 1587–1605. https://doi.org/10.1002/2013JA019204

Ozeke, L. G., Mann, I. R., Murphy, K. R., Rae, I. J., Milling, D. K., Elkington, S. R., et al. (2012). ULF wave derived radiation belt radial diffusion coefficients. *Journal of Geophysical Research*, *117*, A04222. https://doi.org/10.1029/2011JA017463

Ozeke, L. G., Mann, I. R., & Rae, I. J. (2009). Mapping guided Alfvén wave magnetic field amplitudes observed on the ground to equatorial electric field amplitudes in space. *Journal of Geophysical Research*, *114*, A01214. https://doi.org/10.1029/2008JA013041

Pokhotelov, D., Rae, I. J., Murphy, K. R., & Mann, I. R. (2016). Effects of ULF wave power on relativistic radiation belt electrons: 8–9 October 2012 geomagnetic storm. *Journal of Geophysical Research: Space Physics*, *121*, 11,766–11,779. https://doi.org/10.1002/2016JA023130

Rae, I. J., Mann, I. R., Murphy, K. R., Ozeke, L. G., Milling, D. K., Chan, A. A., et al. (2012). Ground-based magnetometer determination of in situ Pc4-5 ULF electric field wave spectra as a function of solar wind speed. *Journal of Geophysical Research*, *117*, A04221. https://doi.org/10.1029/2011JA017335

Richardson, J. D., & Paularena, K. I. (1998). The orientation of plasma structure in the solar wind. *Geophysical Research Letters*, *25*(12), 2097–2100. https://doi.org/10.1029/98GL01520

Roederer, J. G., & Zhang, H. (2014). Dynamics of magnetically trapped particles (Vol. 403). https://doi.org/10.1007/978-3-642-41530-2

Rostoker, G., Samson, J. C., Creutzberg, F., Hughes, T. J., McDiarmid, D. R., McNamara, A. G., et al. (1995). Canopus—A ground-based instrument array for remote sensing the high latitude ionosphere during the ISTP/GGS program. *Space Science Reviews*, *71*(1–4), 743–760. https://doi.org/10.1007/BF00751349

Rostoker, G., Skone, S., & Baker, D. N. (1998). On the origin of relativistic electrons in the magnetosphere associated with some geomagnetic storms. *Geophysical Research Letters*, *25*(19), 3701. https://doi.org/10.1029/98GL02801

Saito, T. (1969). Geomagnetic pulsations. *Space Science Reviews*, *10*(3), 319–412. https://doi.org/10.1007/bf00203620

Sandhu, J. K., Yeoman, T. K., James, M. K., Rae, I. J., & Fear, R. C. (2018). Variations of high-latitude geomagnetic pulsation frequencies: A comparison of time-of-flight estimates and IMAGE magnetometer observations. *Journal of Geophysical Research: Space Physics*, *123*, 567–586. https://doi.org/10.1002/2017JA024434

Sarris, T. E., & Li, X. (2017). Geomagnetic activity and local time dependence of the distribution of ultra low-frequency wave power in azimuthal wavenumbers. *Annales Geophysicae*, *35*(3), 629–638. https://doi.org/10.5194/angeo-35-629-2017

Schulz, M., & Eviatar, A. (1969). Diffusion of equatorial particles in the outer radiation zone. *Journal of Geophysical Research*, *74*(9), 2182–2192. https://doi.org/10.1029/JA074i009p02182

Schulz, M., & Lanzerotti, L. J. (1974). *Particle diffusion in the radiation belts: Physics and chemistry in space* (Vol. 7). Berlin Heidelberg: Springer Berlin Heidelberg. https://doi.org/10.1007/978-3-642-65675-0

Southwood, D. J., & Kivelson, M. G. (1990). The magnetohydrodynamic response of the magnetospheric cavity to changes in solar wind pressure. *Journal of Geophysical Research*, *95*(A3), 2301. https://doi.org/10.1029/JA095iA03p02301

Tanskanen, E. I. (2009). A comprehensive high-throughput analysis of substorms observed by IMAGE magnetometer network: Years 1993-2003 examined. *Journal of Geophysical Research*, *114*, A05204. https://doi.org/10.1029/2008JA013682

Thomsen, M. F. (2004). Why Kp is such a good measure of magnetospheric convection. *Space Weather*, *2*, S11004. https://doi.org/10.1029/2004SW000089

Turner, D. L., Shprits, Y., Hartinger, M., & Angelopoulos, V. (2012). Explaining sudden losses of outer radiation belt electrons during geomagnetic storms. *Nature Physics*, *8*(3), 208–212. https://doi.org/10.1038/nphys2185

Waters, C. L., Menk, F. W., & Fraser, B. J. (1991). The resonance structure of low latitude Pc3 geomagnetic pulsations. *Geophysical Research Letters*, *18*(12), 2293–2296. https://doi.org/10.1029/91GL02550

Watt, C. E., Rae, I. J., Murphy, K. R., Anekallu, C., Bentley, S. N., & Forsyth, C. (2017). The parameterization of wave-particle interactions in the Outer Radiation Belt. *Journal of Geophysical Research: Space Physics*, *122*, 9545–9551. https://doi.org/10.1002/2017JA024339

Weimer, D. R., Ober, D. M., Maynard, N. C., Burke, W. J., Collier, M. R., McComas, D. J., et al. (2002). Variable time delays in the propagation of the interplanetary magnetic field. *Journal of Geophysical Research*, *107*(1), 1210. https://doi.org/10.1029/2001JA009102

West, H. I., Buck, R. M., & Walton, J. R. (1972). Shadowing of electron azimuthal-drift motions near the noon magnetopause. *Nature Physical Science*, *204*, 6–7. https://doi.org/10.1038/physci240006a0